

# Different arrival times of CM and CI-like bodies from the outer Solar System to the asteroid belt

Sarah E. Anderson<sup>1\*</sup>, Pierre Vernazza<sup>1</sup> and Miroslav Brož<sup>2†</sup>

<sup>1</sup>LAM, Laboratoire d’Astrophysique de Marseille, Aix Marseille University, 38 rue Frédéric Joliot-Curie, Marseille, 13013, France.

<sup>2</sup>Charles University, Faculty of Mathematics and Physics, Institute of Astronomy, V Holešovičkách 2, Praha, CZ-18200, Czech Republic.

\*Corresponding author(s). E-mail(s): [sarah.anderson@lam.fr](mailto:sarah.anderson@lam.fr);

Contributing authors: [pierre.vernazza@lam.fr](mailto:pierre.vernazza@lam.fr);

[mira@sirrah.troja.mff.cuni.cz](mailto:mira@sirrah.troja.mff.cuni.cz);

†These authors contributed equally to this work.

## Abstract

Understanding the provenance of CI and CM chondrites, the most primitive materials in our meteorite collections, is critical for shedding light on the Solar System’s early evolution [1, 2, 3, 4, 5] and contextualizing findings from recent sample return missions [6, 7]. Here we show that the parent bodies of CM chondrites originate from the Saturn formation region, whereas those of CI chondrites originate essentially from the primordial trans-Uranian disk. Using N-body simulations to investigate the effect of giant planet growth and inward Type-I migration [8, 9], along with the current observed distribution of CM, CI, and comet-like (P types) bodies in the asteroid belt [10], we demonstrate that CI and CM-like bodies must have been implanted at different times in the belt, while CI and comet-like bodies were implanted at the same time. These different implantation periods are imposed by the fact that the gas disk profile entirely governs the radial distribution of bodies implanted by aerodynamic drag in the asteroid belt. A preferred location coincides with the inner edge of a ‘gap’ opened by Jupiter. Saturn’s growth likely drove the migration of CM-like bodies, whereas CI and comet-like bodies were transported at a later stage, during the outward migration of Uranus and Neptune driven by remaining planetesimals. Since CM chondrites are chondrule-rich, it follows that chondrule formation occurred mostly inward of the ice giant’s formation zone ( $\leq 10$  au). A by-product of our simulations is that only CM-like (not CI-like) bodies contributed to the water budget of the telluric planets.

**Keywords:** solar system formation, small bodies, asteroid belt, chondrites

To date, the vast majority of meteorites ( $\geq 99\%$ ) originate from asteroids in orbits between Mars and Jupiter [6, 7]. The challenge of aligning the large chemical, compositional, and isotopic diversity of meteorites with a model of in-situ formation in the asteroid belt has long eluded consensus. Dynamical models have significantly shifted this paradigm, suggesting that main-belt asteroids — hence meteorites — formed over a large range of heliocentric distances [1, 2, 3, 4, 5], from the terrestrial planet formation region to the Kuiper Belt. This view has been progressively supported by meteorite measurements revealing first a dichotomy between carbonaceous and non-carbonaceous chondrites [11, 12, 13] and more recently a further dichotomy among carbonaceous chondrites (CCs), between CIIs and the remaining CCs [14]. Whereas specific formation locations have been proposed for the different CC groups (most CCs: Jupiter-Saturn formation region, CI chondrites: Neptune formation region; [15]) no single dynamical model has been able to correlate these putative formation locations with the current observed compositional distribution of the asteroid belt. Apart from a general consensus that most CCs formed beyond Jupiter —and even this remains to be unambiguously demonstrated—the origin of the diversity among CC groups, including their various formation locations, remains a mystery.

Today, two meteorite classes are over-represented among CC-like asteroids namely CM chondrites (Ch, Cgh-types [16]) and CI chondrites (B, C, Cb, and Cg-types [17, 18, 14, 19, 20]). The parent bodies of these two meteorite classes represent more than 50% of the mass of the asteroid belt (not counting Ceres) [10]. In contrast, the parent bodies of the remaining CC classes (CO, CV, CK) represent a minority ( $\leq 1\%$ ) of all main belt asteroids [10]. The radial distribution of CM- and CI-like bodies in the asteroid belt appear very different (Fig. 1), with CM-like bodies displaying a rather Gaussian, symmetric profile, whereas CI-like bodies display a markedly asymmetric profile. Of great interest, the distribution of CI-like bodies is remarkably similar to that of comet-like P-type asteroids (Fig. 1), suggesting a common origin. A common link between these two asteroid compositions is not new as they were already linked based on spectroscopic and density measurements [21, 22], with a proposed link to interplanetary dust particles (IDPs).

To constrain the formation location of CM- and CI-like bodies, and shed light on the origin of the isotopic dichotomy among CCs [14], we used an orbital model to investigate the injection of planetesimals into the asteroid belt following giant planet growth. We conducted simulations using REBOUND (ref. [23]), consisting of 20,000 test particles each, representing 100-km-sized planetesimals. Our five-planet model was motivated by the works of Nesvorný [8] and Dienno [9] and featured Jupiter, Saturn, an additional ice giant (which is commonly ejected from the solar system), Uranus, and Neptune. Initially, planets were located on low-eccentricity orbits, with Jupiter at 5.4 au and Saturn at the edge of its gap, at 7.3 au. We chose to neglect the influence

of telluric planets, which, having relatively small orbits, require more computation time. We placed Neptune at two different locations, namely in a ‘tight’ configuration at 16.2 au, in a 3:2, 3:2, 3:2, 3:2 resonance chain, or in a ‘wide’ configuration at 20.3 au, in a 3:2, 3:2, 2:1, 3:2 resonance chain [9]. The test particles’ semi-major axes were initialized uniformly between 7 au and 1 au beyond the orbit of Neptune. We then examined the effect of gas profile ( $\Sigma_g$ ), planetary growth timescale ( $\tau_{\text{growth}}$ ), or the viscosity parameter ( $\alpha$ ) on the distribution of planetesimals implanted in the asteroid belt (see SI for more details). Notably, we investigated three different gas profiles: the traditional canonical model with a radial dependency of  $\Sigma_g \propto r^{-0.5}$  [24], the Desch [25] model, and the Raymond & Izidoro [26] model.

We find that the most influential factor for the distribution of objects within the asteroid belt proves to be the gas profile of the protoplanetary disk rather than the formation location of small bodies, the giant planet growth timescales, the viscosity parameter of the disk, or the configuration of the planets. The final distribution of objects successfully implanted in the asteroid belt strongly reflects the shape of the gas profile (Fig. 2). We tested our hypothesis further by simulating pressure bumps within the protoplanetary disk, by introducing gas profiles characterized by Gaussian peaks. These artificial constructs highlight the paramount importance of the gas profile in the final distribution of planetesimals interior to Jupiter, regardless of their origin: bodies formed around Saturn will end up with the same radial distribution as those that originate around Neptune. Whatever the gas profile, it is interesting to note a small inward radial shift of implanted bodies relative to the gas distribution (Fig. 2).

In the absence of giant planet migration, the vast majority (> 90%, see Tab. 1) of small bodies captured in the asteroid belt originate from the Saturn region (defined as  $a_{\text{ini}} < 10$  au), regardless of the positioning or growth timescales of the ice giants. In all simulations where the gas surface density exceeds  $\sim 10 \text{ g/cm}^2$  in the 10-20 au heliocentric range, however, the interaction between ice giant embryos and the disk gas inevitably leads to their inward migration, dictated by angular momentum exchange with the protoplanetary disk [27, 28]. As a result, we have a migration component in our simulations, most prominent in the ‘wide’ planetary configuration (Fig. 3): Neptune and Uranus spiral inwards as they grow, in some cases reaching almost 12 au. This is most notable in rapid planet formation scenarios ( $\tau_{\text{growth}} = 1 \times 10^5 \text{ yr}$ ). The migrating nascent Uranus and Neptune significantly influence the redistribution of planetesimals towards the asteroid belt, to the extent that, at 300 kyr, a little over half of our implanted objects originate from the >10 au region. This underscores that the most efficient driver of the implantation process from the ice giant region is not planetary growth, but migration. Despite their varied origins, the final distribution of objects in the asteroid belt is almost identical to that of bodies originating from the Saturn region (Fig. 6), with a slight trend to lower heliocentric distance.

Using a Kolmogorov-Smirnov (KS) test, we compared the distributions of each of our final populations with the observed distributions of CM-like bodies by normalizing the cumulative distributions of the semi-major axis at the 3.2 au gap in the inner

belt (Fig. 6). Among our simulations based on synthetic gas profiles, the best-fitting simulation is the one where we forced the gas profile to include a Gaussian pressure bump at a heliocentric distance of 2.7, 2.8, or alternatively 3.0 au. This would seem to indicate that there was a pressure bump of some kind acting as a planetesimal trap in the vicinity of  $\sim$ 2.8 au during the CM implantation period, i.e., Saturn’s growth period. We can think of two mechanisms that could create a pressure bump: The first is a result of the buildup around the water ice line, which was in this vicinity at  $\approx$ 1 Myr after CAIs [29] or a little further out [30]. However, thermal evolution models imply that CM chondrites formed 3-4 Myrs after CAIs [31], at a time when the water ice line had been in the terrestrial region [32]. Alternatively, this pressure bump could also simply be the interior edge of Jupiter’s gap: if this was the case, the distribution of CMs represents a snapshot of Jupiter’s gap at the moment they were implanted in the belt. Finally, none of the gas profiles retrieved from the literature are able to reproduce the asymmetric distribution of CI-like bodies. We ran KS tests also on the cumulative distributions of eccentricities and inclinations, both favored gas profiles with Gaussian pressure bumps, however, these elements were usually damped (as in refs. [5, 33]), which strongly suggests an early gas dispersal or an additional excitation mechanism (see, e.g., [34]).

Overall, our numerical simulations imply that the distribution of small bodies successfully implanted in the asteroid belt mirrors the gas distribution profile of the protoplanetary disk at that time (see Fig. 2). The direct consequence is that the parent bodies of CM and CI chondrites were not implanted into the asteroid belt simultaneously: If they had been, we would expect to observe similar distributions, yet they are markedly distinct (Fig. 1). Contrary to previous beliefs, the original formation location of small bodies (e.g., 10 au versus 20 au) plays a minimal role — per se — in the final distribution in the asteroid belt, for a given ejection time. Rather, the time when they left their birthplace for the asteroid belt is the determining factor.

In the absence of precise knowledge of the actual gas profile of the protosolar disk in the 3-10 Myr time window after CAIs, and its evolution over such interval, we need to rely on other modeling and observational constraints to determine the most likely formation locations of CM and CI chondrites. These include but are not limited to: i) the current distribution of CM, CI and comet-like (P-type) bodies in the inner solar system (Fig. 1); ii) the current 1.1:1 CI/CM ratio in the asteroid belt (Fig. 1); iii) the similar building blocks for CI chondrites and cometary material such as IDPs ( $\sim$ 100% matrix,  $\sim$ 0% chondrules,  $\sim$ 0% CAIs; [35]); iv) the comet-like spectral properties of anhydrous areas in CI chondrites [36]; v) the formation time of CM chondrites (3-4 Myrs after CAIs [31]) and comet-like bodies and TNOs ( $\geq$  4-5 Myrs after CAIs, [37, 31, 38]); vi) the similarity in spectral properties between P/D-type asteroids, Jupiter Trojans, comets and Centaurs [39]; vii) the likely late formation of Uranus and Neptune (4-6 Myrs after CAIs; [40, 41]); viii) the success of the Nice model in explaining many of the observed properties of the solar system (the secular tilt resonance within the cold Edgeworth-Kuiper belt observed today [42], our current planetary configuration, and the capture of Jupiter Trojans and irregular

satellites [34]), including a trans-Neptunian origin for P/D-type asteroids and Jupiter Trojans; ix) the asymmetric distribution of bodies implanted in the asteroid belt following the Nice model, a common property with the present distribution of CI and P-type bodies [43]; and x) the size distribution of TNOs which goes up to  $D \approx 2400$  km (Pluto) instead of  $D \approx 270$  km (diameter of the largest inner solar system P/D-type; [22]) making it highly unlikely that no  $D \geq 300$  km bodies were trapped in the asteroid belt following the outward migration of Uranus and Neptune as described in the Nice model. Yet, the Nice model considers only P and D-type asteroids as former TNOs [3, 43]. Considering CI-like bodies along with P/D-type asteroids as implanted TNOs would help to solve this serious issue [22].

From this set of constraints, synthesized in Fig. 4 for clarity, there is only one satisfactory solution regarding the formation locations of CM and CI chondrites, namely the Saturn formation region for CM chondrites and the region beyond Uranus and up to Neptune's current position (30 au) for CI chondrites. CMs were likely implanted during the phase of Saturn's growth at the inner edge of Jupiter's gap. The current distribution of CM-like bodies in the asteroid belt would thus represent the gas profile that was present at the time of this implantation process, and give us a likely indication of the location of Jupiter's gap, a pressure bump in the gas profile being required to reproduce the current CM distribution. CI and IDP-like P/D-types were implanted at a later stage, following the final outward migration of Uranus and Neptune [44, 1, 45], a period characterized by a significantly depleted gas profile, potentially even after gas dispersal. The absence of gas in the disk would lead to an asymmetric distribution of implanted bodies, akin to that of CI-like and P-type bodies [43] (Fig. 1).

A challenge remains in reproducing the currently similar distributions in eccentricity and inclination (both in excited states) of CI and CM-like bodies (Fig. 3). Note that this property can be extended to other taxonomic classes, S-type asteroids in particular. In contrast, our simulations resulted in a distribution pattern that is notably more orderly and less dynamically excited. Additionally, our simulations find themselves with too much mass outward ( $\sim 3.5$  au) of Jupiter's 2:1 resonance, compared to what is observed. These two trends are a recurrent issue for all simulations performed at a time when gas is still present in the disk [5, 26, 46, 15]. This discrepancy between our simulations and current observational data suggests the presence of an additional, post-implantation dynamical process. Such an event could well be the jump of Jupiter from 5.4 to 5.2 au [47], during the final outward migration of Uranus and Neptune (cf. Nice model). The jump would have excited all objects in the belt in the same way while drastically reducing the number of objects beyond Jupiter's 2:1 resonance.

Our study has important implications regarding the origin of chondrules (once molten, spherical silicate droplets with diameters of 0.2–2 mm), which are an essential component of most undifferentiated meteorite classes. Currently, there are two main theories for their origin, namely a nebular origin or a planetary origin (e.g., [35]). Constraining their birthplace would be a major step forward towards deciphering the

main physical process responsible for their formation. Here, we have shown that the parent bodies of chondrule-poor CM chondrites (20-40% chondrules in volume; [35]) likely formed in the Saturn formation region, whereas the parent bodies of chondrule-free CI chondrites (0% chondrules) likely formed beyond Uranus. Considering that the parent bodies of chondrule-rich enstatite chondrites (ECs) and ordinary chondrites (OCs) ( $\geq 80\%$  chondrules in volume; [35]) certainly formed inward of Jupiter, including in the terrestrial region (in the case of ECs), this implies that chondrule formation occurred mostly inward of the ice giant's formation zone ( $\leq 10$  au), with increased efficiency (in volume % w.r.t. matrix) towards smaller heliocentric distances. This constraint will have to be reproduced in future models aiming to explain the formation process of chondrules.

Finally, our most successful simulations regarding the current distribution of CM-like bodies in the asteroid belt imply that up to 1.5% of CM-like bodies from the source region should have ended up in the formation region (0.4-2 au) of the terrestrial planets. This is an unavoidable consequence of their arrival in the asteroid belt. If the expected mass of planetesimals between Saturn and Uranus is of the order of  $\sim 1 M_{\oplus}$  (see Methods), the average water content of CM-like materials is 10% [48], the amount of water implanted among terrestrial planets should be  $\sim 10^{-3} M_{\oplus}$ . This is compatible with the Earth ocean,  $2.3 \times 10^{-4} M_{\oplus}$ , including also a non-negligible water content in the mantle (2-8 Earth oceans; ref. [49]). Moreover, the D/H ratio of the standard mean ocean water (i.e.,  $1.5 \times 10^{-4}$ ; [50]) is compatible with a CM-like reservoir [51]. It follows that CM-like bodies were the main exogenous source of water to Earth and the telluric planets.

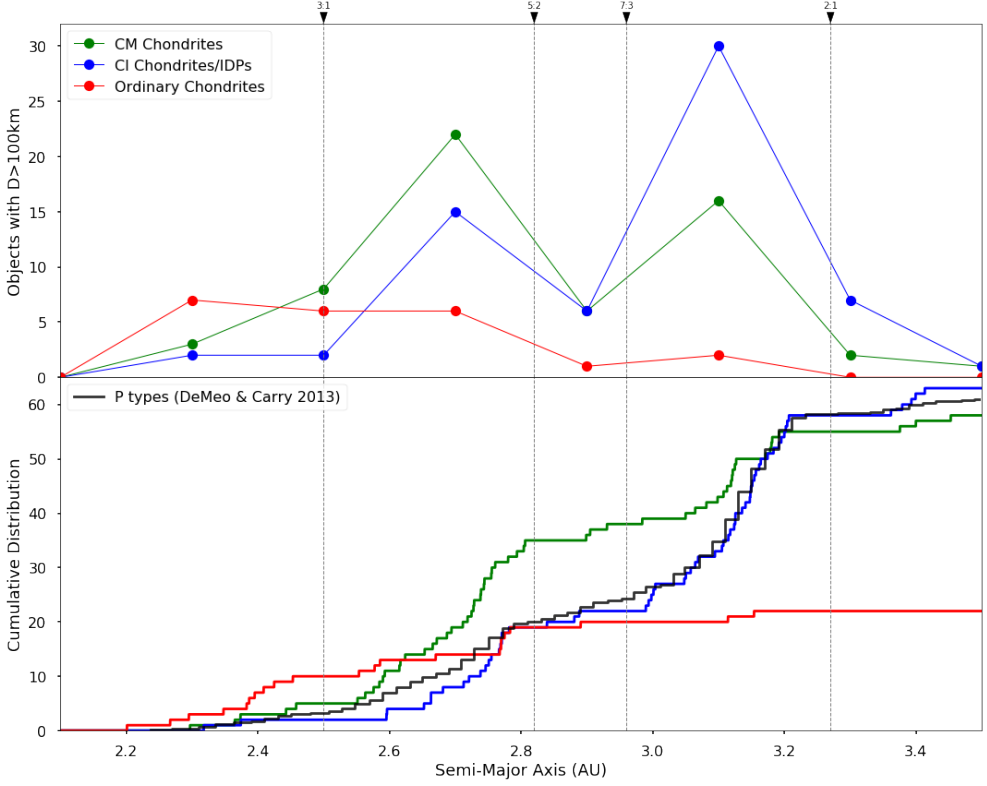


**Fig. 1** Observed distributions of  $>100$  km main-belt asteroids with distinct spectral classifications (CM, CI/IDP, B, S) are systematically different. Top: The number of asteroids classified as chondrule-rich CM (green), chondrule-poor CI/IDP and B-type possessing an albedo below 0.1 (blue), and S-type ordinary-chondrite asteroids (red). We prioritize numerical frequency over mass distribution, a decision driven by the fact that Ceres alone constitutes approximately 90% of the asteroid belt's total mass. To ensure statistical integrity in our evaluations, asteroid families are considered as singular entities, thereby preventing potential overcounts. Bottom: Cumulative distributions of the semimajor axis  $N(\leq a)$  for the same classes of asteroids. For P-types, all  $>30$  km asteroids were included [10], as there are only a dozen P-types  $>100$  km. These are normalized to the number of CI/IDPs at 3.2 au. The positions of major mean-motion resonances with Jupiter (3:1, 5:2, 7:3, 2:1) are indicated by dotted lines. Whereas the distributions of CMs and CI/IDPs are different, CI/IDPs and P-types seem to be compatible according to the Kolmogorov–Smirnov test.

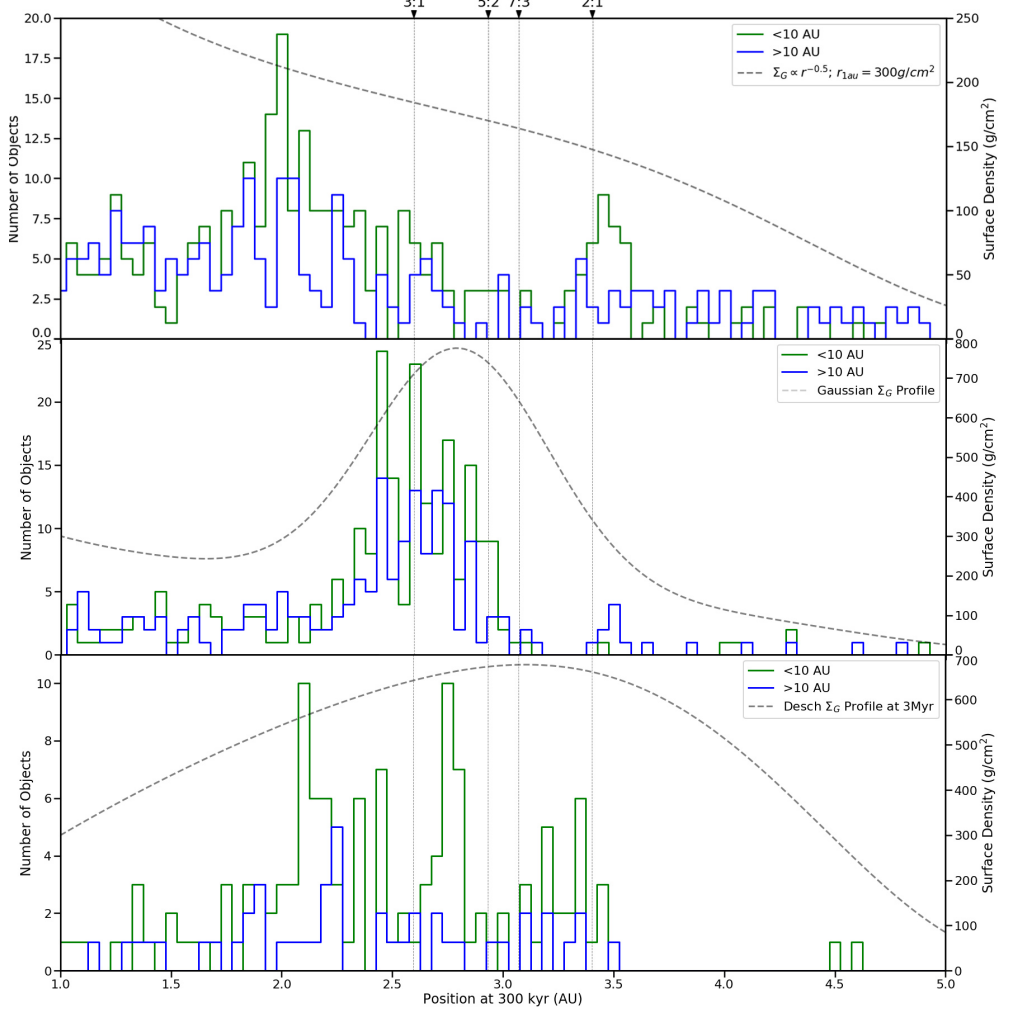


**Fig. 2** Simulated planetesimals implanted by aerodynamic drag closely follow a gas profile of the protoplanetary disk. The semimajor axis distributions of planetesimals implanted interior to Jupiter (solid lines), along with corresponding gas surface density  $\Sigma_g(r)$  (dashed lines). The planetesimals are split into those having formed or originated  $< 10$  au (green) and  $> 10$  (blue). Three different profiles are shown: the canonical model (top), the model with a pressure bump represented by a Gaussian peak (middle), and the gas profile of Desch at 3 Myr [25] (bottom). The simulated time span was 300 kyr. Pressure bumps act as efficient planetesimal traps. As their position subsequently changes, planetesimals are implanted at different locations.

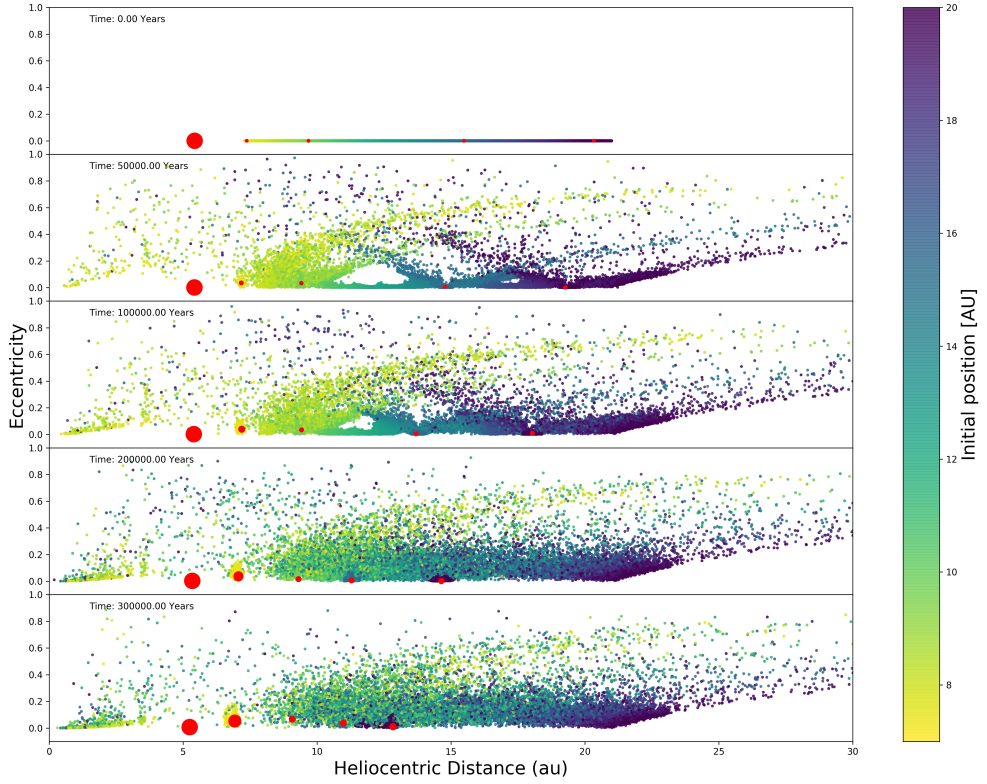


**Fig. 3 Migration of ice giants contributes significantly to the implantation of planetesimals into the asteroid belt.** The temporal evolution of our five-planet system (red) and 20000 planetesimals (multicolored). The heliocentric distance versus eccentricity is shown at the simulation time 0, 0.5, 1, 2, and  $3 \times 10^5$  years. The colours of planetesimals correspond to their original locations. The initial configuration of protoplanets was ‘wide’ (see Tab. 1). The final configuration of the solar system will be attained later, during or after gas dispersal. The canonical gas profile (with the surface density  $\Sigma_g = 300\text{g/cm}^2$  at 1 au) was assumed here. While the growth of the ice giants certainly contributes to the implantation into the asteroid belt, only migration allows for the 1.1:1 CI/CM ratio observed today.

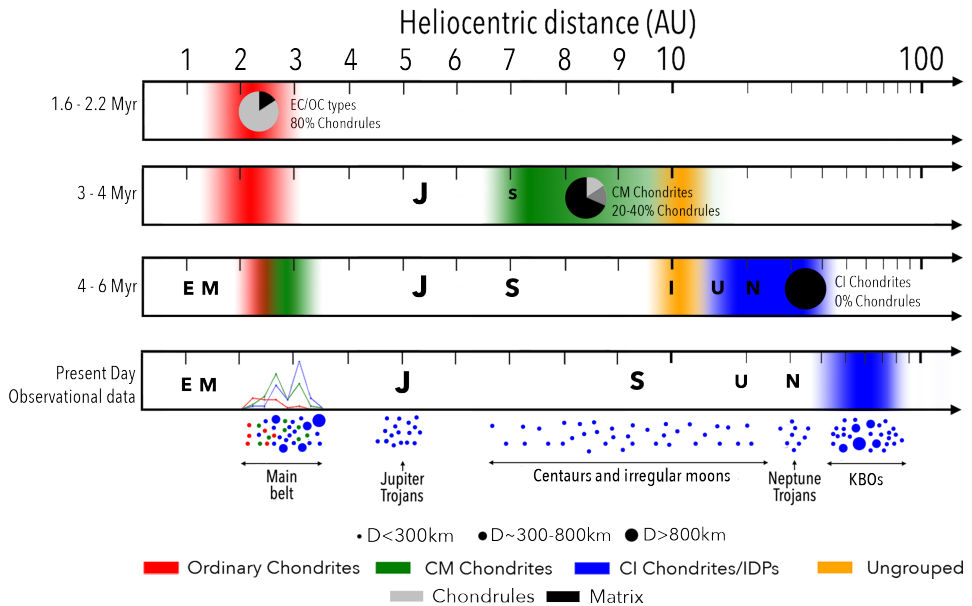


**Fig. 4** Illustration of the heliocentric distribution of different chondritic materials and their dynamical evolution over time. Three important stages can be distinguished: 1.6-2.2 Myr (after the formation of CAIs), 3-4 Myr, and 4-6 Myr, showcasing the temporal and spatial spread of Ordinary Chondrites (red), CM Chondrites (green), and CI Chondrites (blue). Pie charts reflect chondrule content of these bodies. The bottom panel compares the present-day observational data of the asteroid belt and of other populations such as Jupiter Trojans, Centaurs, Neptune Trojans, and Kuiper Belt Objects (KBOs). The circle diameter denotes their typical size. Our model explains the implantation of CM chondrite planetesimals from the Saturn region.

**Table 1** Initial conditions and results of 24 of our simulations after 300 kyr. The ‘wide’ planetary configuration corresponds to Jupiter at 5.4 au, Saturn at 7.3 au, an additional ice giant at 9.7 au [8, 9], Uranus at 15.4 au, and Neptune at 20.3 au. The ‘tight’ configuration places Uranus at 12.2 au and Neptune at 16.2 au. We used a  $\sigma$  of 0.2 au for our narrow Gaussian profiles, while those marked with \* used a  $\sigma$  of 0.4 au. For each simulation, percentages of planetesimals implanted and the corresponding efficiencies were determined.

Gas Profile	Growth Timescale (yr)	Viscosity $\alpha$	Planet Orbit	Implanted by Saturn (%)	Saturn Efficiency (%)	Ice-Giant Efficiency (%)
300 g cm <sup>-2</sup> at 1 au	$5 \times 10^5$	$2 \times 10^{-3}$	Wide	64	2.13	0.30
300 g cm <sup>-2</sup> at 1 au	$1 \times 10^6$	$2 \times 10^{-3}$	Wide	80	1.63	0.10
300 g cm <sup>-2</sup> at 1 au	$1 \times 10^5$	$2 \times 10^{-3}$	Wide	55	2.50	0.51
300 g cm <sup>-2</sup> at 1 au	$5 \times 10^5$	$2 \times 10^{-3}$	Tight	90	1.79	0.08
300 g cm <sup>-2</sup> at 1 au	$1 \times 10^6$	$2 \times 10^{-3}$	Tight	74	1.88	0.17
300 g cm <sup>-2</sup> at 1 au	$1 \times 10^5$	$2 \times 10^{-3}$	Tight	55	2.27	0.45
300 g cm <sup>-2</sup> at 1 au	$5 \times 10^5$	$2 \times 10^{-3}$	No Mig.	93	2.45	0.05
300 g cm <sup>-2</sup> at 1 au	$5 \times 10^5$	$5 \times 10^{-4}$	Wide	67	2.02	0.25
300 g cm <sup>-2</sup> at 1 au	$5 \times 10^5$	$1 \times 10^{-4}$	Wide	67	2.48	0.13
30 g cm <sup>-2</sup> at 1 au	$5 \times 10^5$	$2 \times 10^{-3}$	Wide	88	0.23	0.01
200 g cm <sup>-2</sup> at 1 au	$5 \times 10^5$	$2 \times 10^{-3}$	Wide	76	1.57	0.13
400 g cm <sup>-2</sup> at 1 au	$5 \times 10^5$	$2 \times 10^{-3}$	Wide	61	3.20	0.51
Gaussian at 2.4 au	$5 \times 10^5$	$2 \times 10^{-3}$	Tight	75	4.13	0.60
Gaussian at 2.7 au	$5 \times 10^5$	$2 \times 10^{-3}$	Tight	72	4.33	0.71
Gaussian* at 2.8 au	$5 \times 10^5$	$2 \times 10^{-3}$	Tight	60	5.54	1.55
Gaussian at 3.0 au	$5 \times 10^5$	$2 \times 10^{-3}$	Tight	76	5.10	0.67
Gaussian* at 3.0 au	$5 \times 10^5$	$2 \times 10^{-3}$	Tight	62	6.06	1.59
Gaussian at 3.2 au	$5 \times 10^5$	$2 \times 10^{-3}$	Tight	71	4.83	1.33
Desch 2 Myr	$5 \times 10^5$	$2 \times 10^{-3}$	Tight	79	6.67	0.77
Desch 3 Myr	$5 \times 10^5$	$2 \times 10^{-3}$	Wide	86	3.79	0.11
Desch 3 Myr	$5 \times 10^5$	$2 \times 10^{-3}$	Tight	74	4.47	0.69
Desch 5 Myr	$5 \times 10^5$	$2 \times 10^{-3}$	Tight	75	3.90	0.55
Raymond & Izidoro	$5 \times 10^5$	$2 \times 10^{-3}$	Wide	86	3.00	0.13
Raymond & Izidoro	$5 \times 10^5$	$2 \times 10^{-3}$	Tight	56	1.50	0.50

## Methods

We performed orbital simulations using the open source library `REBOUND`, a well-established N-body integrator [23], selecting the high-accuracy non-symplectic integrator with an adaptive timestepping (IAS15). Each simulation included 20,000 test particles as planetesimals, and the orbits were integrated with a timestep of  $10^{-2}/(2\pi)$  yr. `REBOUND` automatically handles collisions of test particles with the planets by removing them from the simulation to save computation time. Test particles are also removed if their trajectory becomes hyperbolic.

### Giant planet dynamics and growth

As Jupiter reached approximately  $20 M_{\oplus}$ , it had started to create a pressure bump, isolate pebbles from itself [52], and open a gap in the gaseous disk [53, 54, 55]. After fully opening the gap, small-body populations became separated and Jupiter's migration slowed down. This slowing allowed for a steady accumulation of pebbles over time as pebbles became trapped at its gap's outer edge [56], and subsequently accreted into planetesimals. This area of accumulation likely had an increased dust-to-gas ratio, creating conducive conditions for the emergence of larger planetesimals, either through direct cohesion or gravitational instability. Over time, a considerable planetesimal reservoir would have developed at the edge of this gap, with the planet's immediate surroundings remaining relatively barren of solid material. This reservoir's potential significance is underlined by Kobayashi et al. (2012) [57], who postulated that Saturn's core might have formed at Jupiter's gap's outer boundary, a notion echoed by Lambrechts et al. (2014) as it is now clear that Saturn once orbited closer to Jupiter than its present position [9]. With Saturn's subsequent formation at Jupiter's disk boundary, its increasing gravitational influence began to channel objects towards Jupiter and the inner Solar System, while also likely providing the material foundation for the creation of the Galilean moons by adding solids to Jupiter's circumplanetary disk (CPD) [58]. Two prominent populations result from this scattering: those trapped on stable orbits within the asteroid belt and those scattered past the belt toward the terrestrial planets, potentially contributing water to nascent terrestrial planets [59]. The prevalence of each outcome is influenced by the intensity of the gas drag [26], contingent on two main factors: the volumetric density of the gaseous disk, which naturally decreases over time, and the size of the planetesimals, with smaller ones experiencing a heightened drag effect or headwind. Consequently, enhanced gas drag tends to favor implantation, while diminished drag intensifies scattering [46].

Our model consists of five planets: Jupiter, Saturn, and three ice giants, including Uranus, and Neptune. An additional ice giant ("Ice 1") is needed to stabilize the system after the instability [8, 9]. We also chose to neglect the influence of the inner planets, which, having relatively small orbits, require more integration steps and longer calculations.

All planets interact with each other as well as the gas in the disk. Their configuration is dictated by its resemblance to the current Solar System and the observed orbital structure of the trans-Neptunian objects. Our first configuration is 'wide', with the planets in a 3:2, 3:2, 2:1, 3:2 multi-resonance configuration following Deienno et

al. (2017) [9], as this configuration has been shown to introduce the secular tilt resonance within the cold Edgeworth-Kuiper belt observed today [42] as well as many other constraints, such as our current planetary configuration, and the capture of Jupiter Trojans and irregular satellites [34]. In the latter stages of Solar System formation, as gas depletes from the disk, ‘‘Ice 1’’ would be expelled during the Jumping Jupiter phase [47]. Thus, we place Jupiter at a heliocentric distance of approximately 5.4 au, consistent with the post-circumsolar disk dynamical evolution of giant planets. We place Saturn’s core at the edge of Jupiter’s gap, at 7.3 au. Following Deienno et al. (2017) [9], ‘‘Ice 1’’s core is placed at 9.7 au, Uranus’s at 15.4 au, and Neptune’s at 20.3 au. Neptune migrates more or less in the disk as a result of its interaction with the gas. We thus chose to run also simulations with a ‘tight’ configuration, with the cores of Uranus at 12.6 au, and Neptune at 16.2 au in a 3:2, 3:2, 3:2, 3:2 resonance chain. We based our configurations on models that have been shown to work once gas had been removed from the disk. In principle, it is possible for these planetary cores to migrate during their formation while gas remains, before assuming the positions that will lead to the Jumping Jupiter configuration.

Jupiter is assumed to have acquired essentially its current mass ( $\approx 300 M_{\oplus}$ ) before we even begin our simulations, while the four remaining protoplanets or planetary cores are initialized at  $1 M_{\oplus}$ . Their masses incrementally increase linearly over a parametrized timescale,  $\tau_{\text{growth}}$ , as described by:

$$M_{\text{planet}}(t) = M_i + \Delta M (1 - e^{-t/\tau_{\text{growth}}}) , \quad (1)$$

where  $M_i$  is the initial mass of the core and  $\Delta M$  is the difference between the initial core mass and the final mass of each planet. This approach from Ronnet et al. (2018) [58] simplifies the traditional core accretion model, where an envelope contracts, followed by an accelerating and then decelerating gas accretion as a planet forms a gap in the disk [60]. We test different values of  $\tau_{\text{growth}}$  set to  $1 \times 10^5$ ,  $5 \times 10^5$ , and  $1 \times 10^6$ , in order to see what effect this may have on the motion of the surrounding planetesimals. We use  $\tau_{\text{growth}} = 5 \times 10^5$  for our canonical model. While a deeper analysis is needed for accurate growth patterns, the growth trajectories and order of formation of the ice giants remain complex and are not the primary focus of this study.

In each case, we included the eccentricity damping of the giant planets due to interaction with the gas disk using fictitious forces. The effects of aerodynamic drag and eccentricity and semi-major axis damping are included in our simulations following Ronnet et al. (2018) [58], based on the work of Cresswell & Nelson (2008) [24]. We included the effects of eccentricity and semi-major axis damping of the planets due to interactions with the gas disk through the following acceleration terms:

$$\mathbf{a}_{\text{mig}} = -\frac{\mathbf{v}}{\tau_{\text{mig}}} , \quad (2)$$

$$\mathbf{a}_e = -2 \frac{(\mathbf{v} \cdot \mathbf{r}) \mathbf{r}}{r^2 \tau_e} , \quad (3)$$

$$\mathbf{a}_i = -\frac{v_z}{t_i} \mathbf{k} , \quad (4)$$

where  $\mathbf{v}$  is the velocity vector of the planet,  $\mathbf{r}$  is its position vector,  $\mathbf{k}$  is the unit vector in the  $z$ -direction, and  $r$  is the distance to the star. In the case of Saturn, “Ice 1”, Uranus, and Neptune, the eccentricity damping timescale  $\tau_e$  was taken to be  $0.01\tau_{\text{mig}}$  [54]. As we did not consider any radial migration of Jupiter, we always used an eccentricity damping timescale of  $\tau_e = 5 \times 10^3$  years and no semi-major axis damping for this planet. The inclination damping time  $t_i$  is given by:

$$t_i = \frac{t_{\text{wave}}}{0.544} \times \left[ 1 - 0.33 \left( \frac{i}{h} \right)^2 + 0.24 \left( \frac{i}{h} \right)^3 + 0.14 \left( \frac{e}{h} \right)^2 \left( \frac{i}{h} \right) \right], \quad (5)$$

with

$$t_{\text{wave}} = \frac{M_*}{m_p} \frac{M_*}{\Sigma_p a_p^2} h^4 \Omega_p^{-1}, \quad (6)$$

where  $i$  denotes the inclination,  $e$  the eccentricity,  $h \equiv H/r$  the aspect ratio,  $M_*$  the stellar mass,  $m_p$  the planet mass,  $a_p$  its semimajor axis, and  $\Omega_p$  the Kepler frequency.

We neglected possible contribution from heating torque from hot/accreting protoplanets [61], torque modifications at non-zero eccentricity [62], or eccentricity and inclination forcing by the hot-trail effect [63, 64, 65].

These are simplified prescriptions that do not take into account the actual structure of the disk (cf. [66, 67]), as the purpose of this study is not to investigate the precise migration of the giant planets within the disk, but to study implantation of small bodies at specific locations.

## Small body dynamics

Most of the small bodies of the outer Solar System originated from the region between Jupiter and  $\sim 30$  au [68, 69, 44, 70]. Here, we are interested in the behavior of objects formed beyond Jupiter. With this in mind, we limit our simulations to planetesimals formed in the  $7 < a < a_{\text{Neptune}} + 1$  au range, where  $a$  is the initial semi-major axis of our test particles. Our model assigns an equal quantity of planetesimals across each semimajor axis segment, not to mirror the actual, unknown distribution but to ensure comprehensive coverage of potential source regions. Variations in the distribution of planetesimals would not significantly alter the likelihood of their implantation into the asteroid belt [26], as interactions between planetesimals are minimal compared to those between planetesimals and planets or gas. The exact distribution of planetesimals is an interesting problem, as we know from observations of exosystems that a continuous disk at this stage is unlikely, and instead, we would have rings of planetesimals around the star resulting from the pressure bumps formed around icelines and other sublimation lines [30].

We accounted for the aerodynamic drag effects on the planetesimals using the methods described by Ronnet et al. (2017, 2018) [71, 58], by applying the following acceleration term:

$$\mathbf{a}_{\text{drag}} = -\frac{1}{t_s} (\mathbf{v} - \mathbf{v}_g), \quad (7)$$

where  $\mathbf{v}_g$  is the velocity of the gas. The stopping time  $t_s$  is computed using the prescription of Perets & Murray-Clay (2011) [72] and Guillot et al. (2014) [73]:

$$t_s = \left( \frac{\rho_g v_{\text{th}}}{\rho_s R_s} \min \left[ 1, \frac{3}{8} \frac{v_{\text{rel}}}{v_{\text{th}}} C_D \right] \right)^{-1}, \quad (8)$$

where  $R_s$  is the size of the solids, here set to 100 km, and  $\rho_s = 1 \text{ g cm}^{-3}$  their density. The gas volumetric density  $\rho_g$  is obtained from the surface density  $\Sigma_g$  by assuming hydrostatic equilibrium in the vertical direction, with a disk aspect ratio of  $h \equiv H/r = 0.05$  [24]. The relative velocity between the gas and the planetesimal is  $v_{\text{rel}}$ , while the gas thermal velocity is given by  $v_{\text{th}} = \sqrt{8/\pi} c_s$ , where  $c_s$  is the isothermal sound speed. In this context, the isothermal sound speed is defined as  $c_s = \Omega H$ , being  $\Omega$  the Keplerian orbital frequency, expressed as  $\Omega = \sqrt{GM_\odot/r^3}$ . The dimensionless drag coefficient  $C_D$  is computed as a function of the Reynolds number  $\text{Re}$  of the flow around the planetesimal [72]:

$$C_D = \frac{24}{\text{Re}} (1 + 0.27 \text{Re})^{0.43} + 0.47 \left( 1 - e^{-0.04 \text{Re}^{0.38}} \right), \quad (9)$$

$$\text{Re} \equiv \frac{4R_s v_{\text{rel}}}{c_g l_g}. \quad (10)$$

Using the mean free path of the gas  $l_g$  from Supulver & Lin (2000) [74] and the size of 100 km, we find a value of  $C_D = 0.44$ , which is then fixed as a constant to save computational time.

## Gas profiles

The selection of the disk gas profile stands as a notably challenging endeavor in our modeling. Hydrodynamical simulations have been extensively performed over the years (e.g., [75, 76, 77, 78]), each offering nuanced insights and occasionally contrasting perspectives on the gas distribution in protoplanetary disks. These variances arise from the intricate interplay of multiple processes: viscous heating, radiative cooling, stellar irradiation, radiative transfer, dust sublimation, dust settling, and also planet-disk interactions, to name a few. The resultant plethora of potential profiles and the absence of a consensus compel us to make informed yet cautious assumptions when determining the most appropriate gas density profile for our study.

A common result of simplified hydrodynamical disc simulations is to adopt a fixed aspect ratio  $h = 0.05$  and a 1-D surface density profile  $\Sigma_g \propto r^{-0.5}$  [24], normalized so that  $\Sigma_g = 300 \text{ g cm}^{-2}$  at 1 au [58], which corresponds to a moderately evolved disk [76]. We also need to account for the gap opening at Jupiter, which we do by removing a Gaussian centered around Jupiter's orbit with of  $\sigma=1$  au so that the surface density of the gas along Jupiter's orbit is  $10^{-1}$  lower than it would be otherwise. The turbulent viscosity of the disk is parametrized via  $\nu = \alpha c_s^2 \Omega_K$  [79] with  $\alpha$ , the viscous parameter of the disk, typically around  $\alpha = 2 \times 10^{-3}$  for 'dead zones' of the disk.

We also investigate the gas profiles of Desch et al. [25] and Raymond & Izidoro [26] as a point of comparison, as their models were also successful in implanting objects into the asteroid belt.

Desch et al. (2018) [25] initialized the surface density of the gas using a self-similar profile from Hartmann et al. (1998) [80]:

$$\Sigma_g(r, t = 0) = \frac{(2 - \gamma)M_{\text{disk}}}{2\pi R_1} \left( \frac{r}{R_1} \right)^\gamma e^{-\left(\frac{r}{R_1}\right)^{2-\gamma}}, \quad (11)$$

with  $M_{\text{disk}} = 0.089 M_\odot$ ,  $\gamma = 15/14$ , and  $R_1 = 1 \text{ au}$ . The surface density  $\Sigma_g(r, t)$  evolves according to:

$$\frac{\partial \Sigma_g}{\partial t} = \frac{1}{2\pi r} \frac{\partial \dot{M}}{\partial r}, \quad (12)$$

where the mass flux  $\dot{M}$  dependence is determined by:

$$\dot{M} = 6\pi r^{\frac{1}{2}} \frac{\partial}{\partial r} \left( r^{\frac{1}{2}} \Sigma_g \nu \right). \quad (13)$$

The gap at Jupiter might have been opened at approximately 3 au [13]. In our simulations, however, Jupiter's gap is located 5.4 au, since we are examining the effect of Saturn's growth on the implantation efficiency of planetesimals, and, at the same time, most of the CM population is centered around 2.8 au, where an inner edge of Jupiter's gap was possibly located.

Raymond & Izidoro (2017) [26] assumed the surface density profile of Morbidelli et al. (2017) [81], starting after Jupiter and Saturn were both formed. The starting disk profile has a  $\Sigma_g$  of  $200 \text{ g cm}^{-2}$  at 1 au, a gap opened by Jupiter at 5.4 au, and a partial gap opened around Saturn at 7 au. While they decreased the surface density uniformly in radius, on a  $2 \times 10^5 \text{ yr}$  exponential timescale, and removed entirely after  $2 \times 10^6 \text{ yr}$ , we chose to examine their starting disk profile, as the gap opened by Jupiter and Saturn was already much wider than in our profiles.

A comparison of all these gas surface density profiles is shown in Fig. 5.

## Mass of planetesimals disk

The total mass of solids available to form planetesimals and protoplanets is varied among our models. In particular, we were concerned with the mass between Saturn and Uranus, which corresponds to CM-like material. The upper limit is given by integrating the canonical gas profile ( $\Sigma_g$  of  $300 \text{ g cm}^{-2}$  at 1 au) over 7.3 to 15.4 au, in the case of a ‘wide’ configuration of planets. For an assumed metallicity (0.02; based on ref. [82]) this amounts up to  $38 M_\oplus$ . However, a substantial part of this material contributes to the growth of “Ice 1”, Uranus, possibly also Saturn’s core. Since we do not model the growth itself (only parametrically), we should subtract at least 14.5 and  $14.5 M_\oplus$ , so that the remaining planetesimals amount to approximately  $9 M_\oplus$ . The lower limit is given by assuming a ‘tight’ configuration of planets (12.6 au), a lower metallicity (0.01). This would lead to  $12 M_\oplus$ , which seems to be insufficient for the respective planets, nevertheless, we can conclude that the lower limit for the mass of planetesimal disk is of the order of  $\approx 1 M_\oplus$ .

## Arguments against implantation of CI-like bodies

Our simulations revealed an excessive efficiency of implantation for CI bodies. Supposing the total mass of planetesimals in the trans-Uranus region is around  $30 M_\oplus$  — as is

required to drive Neptune's outward migration [83] — 5% would be aerodynamically implanted in the belt. Even if late instabilities depleted this by a factor of 100, the remaining  $0.015 M_{\oplus}$  still exceeds the current asteroid belt mass of  $4 \times 10^{-4} M_{\oplus}$  [84].

Similarly, about 1.5% of CI-like bodies, or  $0.45 M_{\oplus}$ , would be implanted in the terrestrial region. We counted all bodies located among terrestrial planets at 300 ky, given that all orbits have undergone significant damping at this stage. These will be accreted by the terrestrial planets in due course. With an estimated 10% water content [48], the resulting  $0.045 M_{\oplus}$  still exceeds the upper limits for the Earth mantle's water content, up to  $2 \times 10^{-3} M_{\oplus}$  [49].

The only solution to this problem is that CI-like bodies were not implanted during the gas phase, as in ref. [33], but after gas dispersal, with a much lower implantation efficiency of the order of  $4 \times 10^{-6}$  [85]. This results in the correct mass of CI-like bodies (i.e., a quarter of the asteroid belt), and a negligible contribution to the terrestrial planets.

**Acknowledgments.** The work of M.B. has been supported by the Czech Science Foundation (grant number 21-11058S).

**Author contributions.** The authors contributed equally to this work.

**Competing interests.** The authors declare no competing interests.

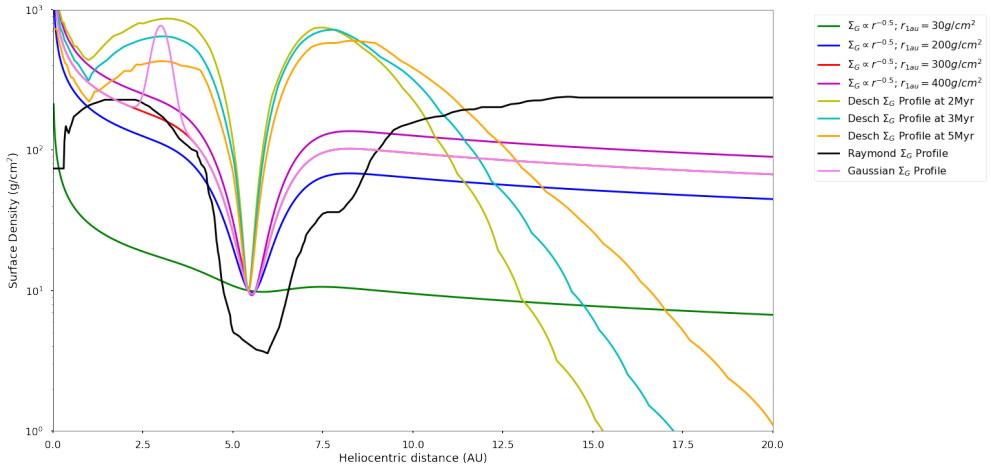


**Fig. 5 A comparison of the different disk profiles used throughout this study.** The surface density  $\Sigma_g(r)$  is plotted as a function of the heliocentric distance  $r$ . We assumed Jupiter has opened a gap in the gaseous disk at approximately 5.4 au. Its current position 5.2 au has been attained at later times, during a gas-free stage. The exact shape of this gap is not very important. We examined the canonical profile, a Gaussian peak approximation (which is valid around 3 au), the Desch [25] profile at different periods, and the initial Raymond [26] profile.

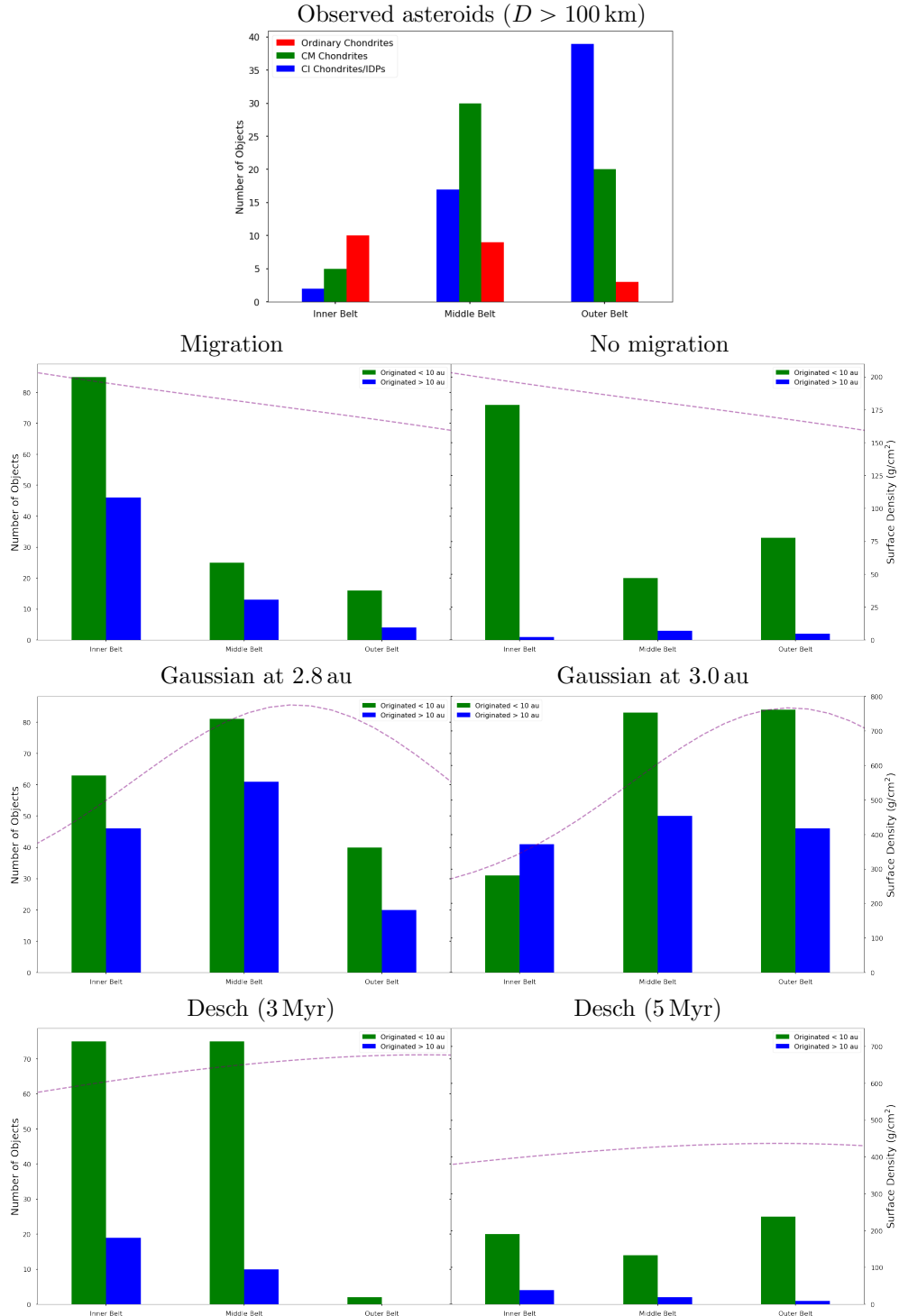


**Fig. 6 Implantation of CM and CI/IDP planetesimals occurred at different times, following the evolution of the gas profile.** The number of planetesimals implanted in the inner, middle, and outer belt (solid lines), along with the corresponding gas surface density  $\Sigma_g(r)$  (dashed lines). In green, the objects successfully implanted in the belt that originally formed at  $< 10$  au, and in blue, those which formed at  $> 10$  au. Above: The observed distributions of ordinary, CM-, and CI-chondrite-like asteroids with  $D > 100$  km in the belt. Top: The canonical model; assuming a wide configuration of planets. The growth timescale of the ice giant planets was  $5 \times 10^5$  yr. At left, the planetary embryos are allowed to migrate inwards due to their interactions with gas. At right, we neglected the interaction with gas and allowed the embryos to grow without migration. Middle: The model with a Gaussian peak; assuming a tight configuration of planets. At left, we changed the gas profile to ensure the peak is located at 2.8 au. At right, at 3.0 au. Bottom: Model with a wide configuration of planets, using the 3 Myr gas profile (left) and 5 Myr gas profile (right) from [25]. The implantation from the Saturn region is always more efficient than from the trans-Uranian region, but both populations end up in near identical distributions, as dictated by the gas profile. This implies that CI/IDPs were implanted at a later time than CMs; possibly during a gas-free stage.

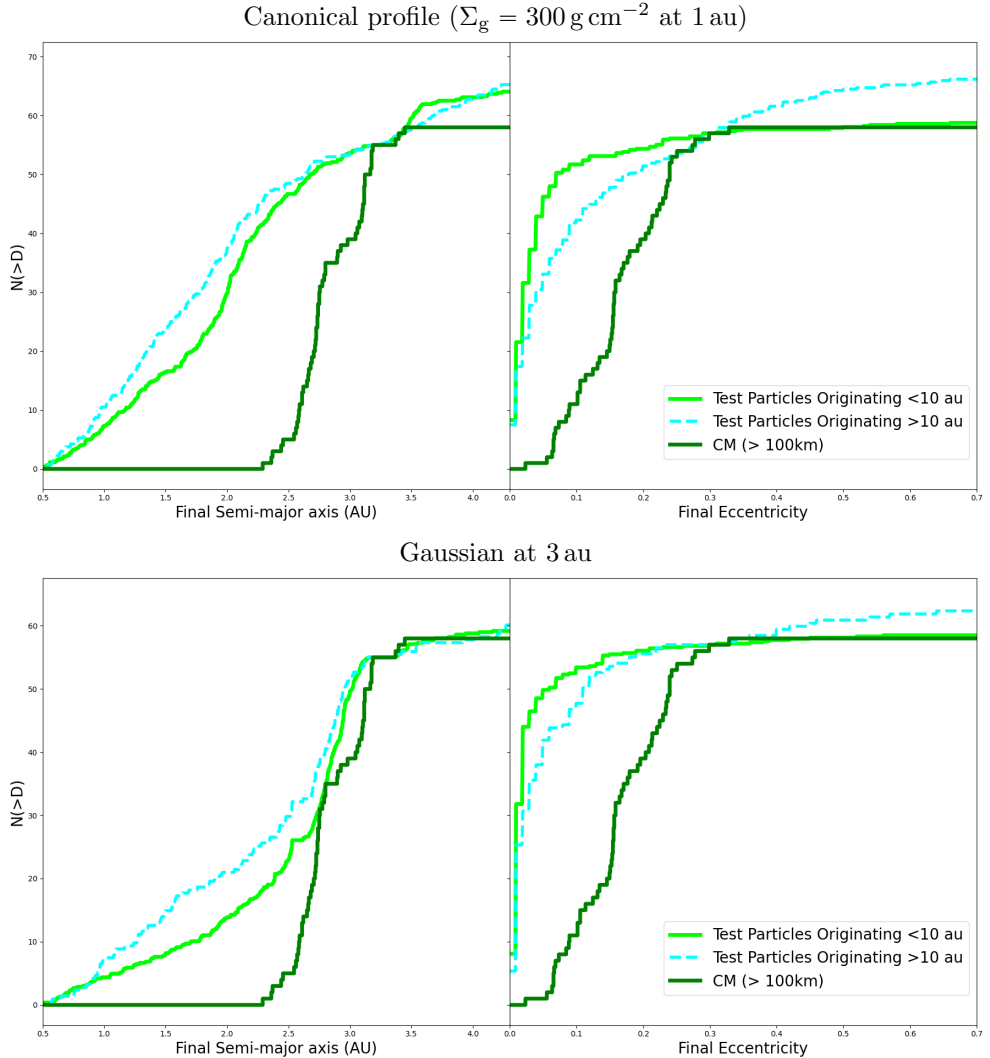


**Fig. 7 A pressure trap in the gas at 2.7 to 3 au would allow planetesimals arriving from Saturn to reach their observed radial distribution.** Cumulative distributions of semi-major axes (left) and eccentricities (right) of our models at 300 kyr simulation time are compared to the observed distribution of CM- (green) and CI- (blue) chondrites. Top: An excluded model with the canonical surface density profile and the tight configuration of planets. Bottom: A preferred model with a Gaussian pressure bump placed at 3.0 au, with a  $\sigma$  of 0.4 au. The arriving planetesimals were split by their origin, with the black line representing those that formed near Saturn ( $< 10$  au). The distributions are normalized to the CM distribution at  $a = 3.2$  au,  $e = 0.3$ . The excess of planetesimals  $< 2$  au compared to what is observed today reveals their contribution to the water content of the terrestrial planets. The main difference between our simulations and the observed distributions is that the eccentricities (and inclinations) are strongly damped. This results from the presence of gas in the disk; it strongly suggests an excitation event occurred after CMs arrived in the belt.

## References

- [1] A. Morbidelli, H. F. Levison, K. Tsiganis, and R. Gomes. Chaotic capture of Jupiter’s Trojan asteroids in the early Solar System. *Nature*, 435(7041):462–465, May 2005.
- [2] William F. Bottke, David Nesvorný, Robert E. Grimm, Alessandro Morbidelli, and David P. O’Brien. Iron meteorites as remnants of planetesimals formed in the terrestrial planet region. *Nature*, 439(7078):821–824, February 2006.
- [3] Harold F. Levison, William F. Bottke, Matthieu Gounelle, Alessandro Morbidelli, David Nesvorný, and Kleomenis Tsiganis. Contamination of the asteroid belt by primordial trans-Neptunian objects. *Nature*, 460(7253):364–366, July 2009.
- [4] Kevin J. Walsh, Alessandro Morbidelli, Sean N. Raymond, David P. O’Brien, and Avi M. Mandell. A low mass for Mars from Jupiter’s early gas-driven migration. *Nature*, 475(7355):206–209, July 2011.
- [5] Sean N. Raymond and Andre Izidoro. Origin of water in the inner Solar System: Planetesimals scattered inward during Jupiter and Saturn’s rapid gas accretion. *Icarus*, 297:134–148, November 2017.
- [6] Michaël Marsset, Pierre Vernazza, Miroslav Brož, Cristina A. Thomas, Francesca E. DeMeo, Brian Burt, Richard P. Binzel, Vishnu Reddy, Allison McGraw, Chrysa Avdellidou, Benoit Carry, Stephen M. Slivan, and David Polishook. The Massalia asteroid family as the origin of ordinary L chondrites. *Nature*, *submit.*, page arXiv:2403.08548, March 2024.
- [7] M. Brož, P. Vernazza, M. Marsset, F. E. DeMeo, R. P. Binzel, D. Vokrouhlický, and D. Nesvorný. Young asteroid families as the primary source of meteorites. *Nature*, *submit.*, page arXiv:2403.08552, March 2024.
- [8] David Nesvorný. Evidence for slow migration of neptune from the inclination distribution of kuiper belt objects. *The Astronomical Journal*, 150(3):73, aug 2015.
- [9] Rogerio Deienno, Alessandro Morbidelli, Rodney S. Gomes, and David Nesvorný. Constraining the Giant Planets’ Initial Configuration from Their Evolution: Implications for the Timing of the Planetary Instability. *Astron. J.*, 153(4):153, April 2017.
- [10] F. E. DeMeo and B. Carry. The taxonomic distribution of asteroids from multi-filter all-sky photometric surveys. *Icarus*, 226(1):723–741, September 2013.
- [11] Paul H. Warren. Stable-isotopic anomalies and the accretionary assemblage of the Earth and Mars: A subordinate role for carbonaceous chondrites. *Earth and Planetary Science Letters*, 311(1):93–100, November 2011.
- [12] Gerrit Budde, Christoph Burkhardt, Gregory A. Brennecka, Mario Fischer-Gödde, Thomas S. Kruijer, and Thorsten Kleine. Molybdenum isotopic evidence for the origin of chondrules and a distinct genetic heritage of carbonaceous and non-carbonaceous meteorites. *Earth and Planetary Science Letters*, 454:293–303, 2016.
- [13] Thomas S. Kruijer, Christoph Burkhardt, Gerrit Budde, and Thorsten Kleine. Age of jupiter inferred from the distinct genetics and formation times of meteorites. *Proceedings of the National Academy of Sciences*, 114(26):6712–6716, 2017.

- [14] Timo Hopp, Nicolas Dauphas, Yoshinari Abe, Jérôme Aléon, Conel M. O'D. Alexander, Sachiko Amari, Yuri Amelin, Ken ichi Bajo, Martin Bizzarro, Audrey Bouvier, Richard W. Carlson, Marc Chaussidon, Byeon-Gak Choi, Andrew M. Davis, Tommaso Di Rocco, Wataru Fujiya, Ryota Fukai, Ikshu Gautam, Makiko K. Haba, Yuki Hibiya, Hiroshi Hidaka, Hisashi Homma, Peter Hoppe, Gary R. Huss, Kiyohiro Ichida, Tsuyoshi Iizuka, Trevor R. Ireland, Akira Ishikawa, Motoo Ito, Shoichi Itoh, Noriyuki Kawasaki, Noriko T. Kita, Kouki Kitajima, Thorsten Kleine, Shintaro Komatani, Alexander N. Krot, Ming-Chang Liu, Yuki Masuda, Kevin D. McKeegan, Mayu Morita, Kazuko Motomura, Frédéric Moynier, Izumi Nakai, Kazuhide Nagashima, David Nesvorný, Ann Nguyen, Larry Nittler, Morihiko Onose, Andreas Pack, Changkun Park, Laurette Piani, Liping Qin, Sara S. Russell, Naoya Sakamoto, Maria Schönbächler, Lauren Tafla, Haolan Tang, Kentaro Terada, Yasuko Terada, Tomohiro Usui, Sohei Wada, Meenakshi Wadhwa, Richard J. Walker, Katsuyuki Yamashita, Qing-Zhu Yin, Tetsuya Yokoyama, Shigekazu Yoneda, Edward D. Young, Hiroharu Yui, Ai-Cheng Zhang, Tomoki Nakamura, Hiroshi Naraoka, Takaaki Noguchi, Ryuji Okazaki, Kanako Sakamoto, Hikaru Yabuta, Masanao Abe, Akiko Miyazaki, Aiko Nakato, Masahiro Nishimura, Tatsuaki Okada, Toru Yada, Kasumi Yogata, Satoru Nakazawa, Takanao Saiki, Satoshi Tanaka, Fuyuto Terui, Yuichi Tsuda, Sei ichiro Watanabe, Makoto Yoshikawa, Shogo Tachibana, and Hisayoshi Yurimoto. Ryugu's nucleosynthetic heritage from the outskirts of the solar system. *Science Advances*, 8(46):eadd8141, 2022.
- [15] David Nesvorný, Nicolas Dauphas, David Vokrouhlický, Rogerio Deienno, and Timo Hopp. Isotopic trichotomy of main belt asteroids from implantation of outer solar system planetesimals. *Earth and Planetary Science Letters*, 626:118521, January 2024.
- [16] P. Vernazza, M. Marsset, P. Beck, R. P. Binzel, M. Birlan, E. A. Cloutis, F. E. DeMeo, C. Dumas, and T. Hiroi. Compositional Homogeneity of CM Parent Bodies. *Astron. J.*, 152(3):54, September 2016.
- [17] Francesca E. DeMeo, Brian J. Burt, Michaël Marsset, David Polishook, Thomas H. Burbine, Benoît Carry, Richard P. Binzel, Pierre Vernazza, Vishnu Reddy, Michelle Tang, Cristina A. Thomas, Andrew S. Rivkin, Nicholas A. Moskovitz, Stephen M. Slivan, and Schelte J. Bus. Connecting asteroids and meteorites with visible and near-infrared spectroscopy. *Icarus*, 380:114971, July 2022.
- [18] Motoo Ito, Naotaka Tomioka, Masayuki Uesugi, Akira Yamaguchi, Naoki Shirai, Takuji Ohigashi, Ming-Chang Liu, Richard C. Greenwood, Makoto Kimura, Naoya Imae, Kentaro Uesugi, Aiko Nakato, Kasumi Yogata, Hayato Yuzawa, Yu Kodama, Akira Tsuchiyama, Masahiro Yasutake, Ross Findlay, Ian A. Franchi, James A. Malley, Kaitlyn A. McCain, Nozomi Matsuda, Kevin D. McKeegan, Kaori Hirahara, Akihisa Takeuchi, Shun Sekimoto, Ikuya Sakurai, Ikuo Okada, Yuzuru Karouji, Masahiko Arakawa, Atsushi Fujii, Masaki Fujimoto, Masahiko Hayakawa, Naoyuki Hirata, Naru Hirata, Rie Honda, Chikatoshi Honda, Satoshi Hosoda, Yu-ichi Iijima, Hitoshi Ikeda, Masateru Ishiguro, Yoshiaki Ishihara, Takahiro Iwata, Kosuke Kawahara, Shota Kikuchi, Kohei Kitazato,

- Koji Matsumoto, Moe Matsuoka, Tatsuhiro Michikami, Yuya Mimasu, Akira Miura, Osamu Mori, Tomokatsu Morota, Satoru Nakazawa, Noriyuki Namiki, Hirotomo Noda, Rina Noguchi, Naoko Ogawa, Kazunori Ogawa, Tatsuaki Okada, Chisato Okamoto, Go Ono, Masanobu Ozaki, Takanao Saiki, Naoya Sakatani, Hirotaka Sawada, Hiroki Senshu, Yuri Shimaki, Kei Shirai, Seiji Sugita, Yuto Takei, Hiroshi Takeuchi, Satoshi Tanaka, Eri Tatsumi, Fuyuto Terui, Ryudo Tsukizaki, Koji Wada, Manabu Yamada, Tetsuya Yamada, Yukio Yamamoto, Hajime Yano, Yasuhiro Yokota, Keisuke Yoshihara, Makoto Yoshikawa, Kent Yoshikawa, Ryota Fukai, Shizuo Furuya, Kentaro Hatakeyama, Tasuku Hayashi, Yuya Hitomi, Kazuya Kumagai, Akiko Miyazaki, Masahiro Nishimura, Hiromichi Soejima, Ayako Iwamae, Daiki Yamamoto, Miwa Yoshitake, Toru Yada, Masanao Abe, Tomohiro Usui, Sei-ichiro Watanabe, and Yuichi Tsuda. A pristine record of outer Solar System materials from asteroid Ryugu's returned sample. *Nature Astronomy*, 6:1163–1171, August 2022.
- [19] Toru Yada, Masanao Abe, Tatsuaki Okada, Aiko Nakato, Kasumi Yogata, Akiko Miyazaki, Kentaro Hatakeyama, Kazuya Kumagai, Masahiro Nishimura, Yuya Hitomi, Hiromichi Soejima, Miwa Yoshitake, Ayako Iwamae, Shizuo Furuya, Masayuki Uesugi, Yuzuru Karouji, Tomohiro Usui, Tasuku Hayashi, Daiki Yamamoto, Ryota Fukai, Seiji Sugita, Yuichiro Cho, Koki Yumoto, Yuna Yabe, Jean-Pierre Bibring, Cedric Pilorget, Vincent Hamm, Rosario Brunetto, Lucie Riu, Lionel Lourit, Damien Loizeau, Guillaume Lequertier, Aurelie Moussi-Soffys, Shogo Tachibana, Hirotaka Sawada, Ryuji Okazaki, Yoshinori Takano, Kanako Sakamoto, Yayoi N. Miura, Hajime Yano, Trevor R. Ireland, Tetsuya Yamada, Masaki Fujimoto, Kohei Kitazato, Noriyuki Namiki, Masahiko Arakawa, Naru Hirata, Hisayoshi Yurimoto, Tomoki Nakamura, Takaaki Noguchi, Hikaru Yabuta, Hiroshi Naraoka, Motoo Ito, Eizo Nakamura, Kentaro Uesugi, Katsuma Kobayashi, Tatsuhiro Michikami, Hiroshi Kikuchi, Naoyuki Hirata, Yoshiaki Ishihara, Koji Matsumoto, Hirotomo Noda, Rina Noguchi, Yuri Shimaki, Kei Shirai, Kazunori Ogawa, Koji Wada, Hiroki Senshu, Yukio Yamamoto, Tomokatsu Morota, Rie Honda, Chikatoshi Honda, Yasuhiro Yokota, Moe Matsuoka, Naoya Sakatani, Eri Tatsumi, Akira Miura, Manabu Yamada, Atsushi Fujii, Chikako Hirose, Satoshi Hosoda, Hitoshi Ikeda, Takahiro Iwata, Shota Kikuchi, Yuya Mimasu, Osamu Mori, Naoko Ogawa, Go Ono, Takanobu Shimada, Stefania Soldini, Tadateru Takahashi, Yuto Takei, Hiroshi Takeuchi, Ryudo Tsukizaki, Kent Yoshikawa, Fuyuto Terui, Satoru Nakazawa, Satoshi Tanaka, Takanao Saiki, Makoto Yoshikawa, Sei-ichiro Watanabe, and Yuichi Tsuda. Preliminary analysis of the Hayabusa2 samples returned from C-type asteroid Ryugu. *Nature Astronomy*, 6:214–220, December 2021.
- [20] Tetsuya Yokoyama, Kazuhide Nagashima, Izumi Nakai, Edward D. Young, Yoshi-nari Abe, Jérôme Aléon, Conel M. O'D. Alexander, Sachiko Amari, Yuri Amelin, Ken ichi Bajo, Martin Bizzarro, Audrey Bouvier, Richard W. Carlson, Marc Chaussidon, Byeong-Gak Choi, Nicolas Dauphas, Andrew M. Davis, Tommaso Di Rocco, Wataru Fujiya, Ryota Fukai, Ikshu Gautam, Makiko K. Haba, Yuki Hibiya, Hiroshi Hidaka, Hisashi Homma, Peter Hoppe, Gary R. Huss, Kiyohiro Ichida, Tsuyoshi Iizuka, Trevor R. Ireland, Akira Ishikawa, Motoo Ito,

- Shoichi Itoh, Noriyuki Kawasaki, Noriko T. Kita, Kouki Kitajima, Thorsten Kleine, Shintaro Komatani, Alexander N. Krot, Ming-Chang Liu, Yuki Masuda, Kevin D. McKeegan, Mayu Morita, Kazuko Motomura, Frédéric Moynier, Ann Nguyen, Larry Nittler, Morihiko Onose, Andreas Pack, Changkun Park, Laurette Piani, Liping Qin, Sara S. Russell, Naoya Sakamoto, Maria Schönbächler, Lauren Tafla, Haolan Tang, Kentaro Terada, Yasuko Terada, Tomohiro Usui, Sohei Wada, Meenakshi Wadhwa, Richard J. Walker, Katsuyuki Yamashita, Qing-Zhu Yin, Shigekazu Yoneda, Hiroharu Yui, Ai-Cheng Zhang, Harold C. Connolly, Dante S. Lauretta, Tomoki Nakamura, Hiroshi Naraoka, Takaaki Noguchi, Ryuji Okazaki, Kanako Sakamoto, Hikaru Yabuta, Masanao Abe, Masahiko Arakawa, Atsushi Fujii, Masahiko Hayakawa, Naoyuki Hirata, Naru Hirata, Rie Honda, Chikatoshi Honda, Satoshi Hosoda, Yuichi Iijima, Hitoshi Ikeda, Masateru Ishiguro, Yoshiaki Ishihara, Takahiro Iwata, Kosuke Kawahara, Shota Kikuchi, Kohei Kitazato, Koji Matsumoto, Moe Matsuoka, Tatsuhiro Michikami, Yuya Mimasu, Akira Miura, Tomokatsu Morota, Satoru Nakazawa, Noriyuki Namiki, Hirotomo Noda, Rina Noguchi, Naoko Ogawa, Kazunori Ogawa, Tatsuaki Okada, Chisato Okamoto, Go Ono, Masanobu Ozaki, Takao Saiki, Naoya Sakatani, Hirotaka Sawada, Hiroki Senshu, Yuri Shimaki, Kei Shirai, Seiji Sugita, Yuto Takei, Hiroshi Takeuchi, Satoshi Tanaka, Eri Tatsumi, Fuyuto Terui, Yuichi Tsuda, Ryudo Tsukizaki, Koji Wada, Seiichiro Watanabe, Manabu Yamada, Tetsuya Yamada, Yukio Yamamoto, Hajime Yano, Yasuhiro Yokota, Keisuke Yoshihara, Makoto Yoshikawa, Kent Yoshikawa, Shizuhiko Furuya, Kentaro Hatakeyama, Tasuku Hayashi, Yuya Hitomi, Kazuya Kumagai, Akiko Miyazaki, Aiko Nakato, Masahiro Nishimura, Hiromichi Soejima, Ayako Suzuki, Toru Yada, Daiki Yamamoto, Kasumi Yogata, Miwa Yoshitake, Shogo Tachibana, and Hisayoshi Yurimoto. Samples returned from the asteroid ryugu are similar to ivuna-type carbonaceous meteorites. *Science*, 379(6634):eabn7850, 2023.
- [21] P. Vernazza, M. Marsset, P. Beck, R. P. Binzel, M. Birlan, R. Brunetto, F. E. Demeo, Z. Djouadi, C. Dumas, S. Merouane, O. Mousis, and B. Zanda. Interplanetary Dust Particles as Samples of Icy Asteroids. *Astrophys. J.*, 806(2):204, June 2015.
- [22] P. Vernazza, M. Ferrais, L. Jorda, J. Hanuš, B. Carry, M. Marsset, M. Brož, R. Fetick, M. Viikinkoski, F. Marchis, F. Vachier, A. Drouard, T. Fusco, M. Birlan, E. Podlewska-Gaca, N. Rambaux, M. Neveu, P. Bartczak, G. Dudziński, E. Jehin, P. Beck, J. Berthier, J. Castillo-Rogez, F. Cipriani, F. Colas, C. Dumas, J. Ďurech, J. Grice, M. Kaasalainen, A. Kryszczynska, P. Lamy, H. Le Coroller, A. Marciniak, T. Michalowski, P. Michel, T. Santana-Ros, P. Tanga, A. Vigan, O. Witasse, B. Yang, P. Antonini, M. Audejean, P. Aurard, R. Behrend, Z. Benkhaldoun, J. M. Bosch, A. Chapman, L. Dalmon, S. Fauvaut, Hiroko Hamanowa, Hiromi Hamanowa, J. His, A. Jones, D. H. Kim, M. J. Kim, J. Krajewski, O. Labrevoir, A. Leroy, F. Livet, D. Molina, R. Montaigut, J. Oey, N. Payre, V. Reddy, P. Sabin, A. G. Sanchez, and L. Socha. VLT/SPHERE imaging survey of the largest main-belt asteroids: Final results and synthesis. *Astron. Astrophys.*, 654:A56, October 2021.

- [23] H. Rein and S. F. Liu. REBOUND: an open-source multi-purpose N-body code for collisional dynamics. *Astron. Astrophys.*, 537:A128, January 2012.
- [24] P. Cresswell and R. P. Nelson. Three-dimensional simulations of multiple protoplanets embedded in a protostellar disc. *Astron. Astrophys.*, 482(2):677–690, May 2008.
- [25] Steven J. Desch, Anusha Kalyaan, and Conel M. O’D. Alexander. The effect of jupiter’s formation on the distribution of refractory elements and inclusions in meteorites. *The Astrophysical Journal Supplement Series*, 238(1):11, sep 2018.
- [26] Sean N. Raymond and Andre Izidoro. The empty primordial asteroid belt. *Science Advances*, 3(9):e1701138, 2017.
- [27] William R. Ward. Protoplanet Migration by Nebula Tides. *Icarus*, 126(2):261–281, April 1997.
- [28] André Izidoro, Alessandro Morbidelli, Sean N. Raymond, Franck Hersant, and Arnaud Pierens. Accretion of Uranus and Neptune from inward-migrating planetary embryos blocked by Jupiter and Saturn. *Astron. Astrophys.*, 582:A99, October 2015.
- [29] Schneeberger, Antoine, Mousis, Olivier, Aguichine, Artyom, and Lunine, Jonathan I. Evolution of the reservoirs of volatiles in the protosolar nebula. *Astron. Astrophys.*, 670:A28, 2023.
- [30] Andre Izidoro, Rajdeep Dasgupta, Sean N. Raymond, Rogerio Deienno, Bertram Bitsch, and Andrea Isella. Planetesimal rings as the cause of the Solar System’s planetary architecture. *Nature Astronomy*, 6:357–366, March 2022.
- [31] Marc Neveu and Pierre Vernazza. IDP-like Asteroids Formed Later than 5 Myr After Ca-Al-rich Inclusions. *Astrophys. J.*, 875(1):30, April 2019.
- [32] Artyom Aguichine, Olivier Mousis, and Jonathan I. Lunine. The Possible Formation of Jupiter from Supersolar Gas. *Planet. Sci. J.*, 3(6):141, June 2022.
- [33] David Nesvorný, Nicolas Dauphas, David Vokrouhlický, Rogerio Deienno, and Timo Hopp. Isotopic trichotomy of main belt asteroids from implantation of outer solar system planetesimals. *Earth and Planetary Science Letters*, 626:118521, January 2024.
- [34] David Nesvorný. Dynamical Evolution of the Early Solar System. *Annu. Rev. Astron. Astrophys.*, 56:137–174, September 2018.
- [35] Robert Hutchison. *Meteorites*. 2004.
- [36] R. Brunetto, C. Lantz, Y. Fukuda, A. Aléon-Toppani, T. Nakamura, Z. Dionnet, D. Baklouti, F. Borondics, Z. Djouadi, S. Rubino, K. Amano, M. Matsumoto, Y. Fujioka, T. Morita, M. Kukuri, E. Kagawa, M. Matsuoka, R. Milliken, H. Yurimoto, T. Noguchi, R. Okazaki, H. Yabuta, H. Naraoka, K. Sakamoto, S. Tachibana, T. Yada, M. Nishimura, A. Nakato, A. Miyazaki, K. Yogata, M. Abe, T. Okada, T. Usui, M. Yoshikawa, T. Saiki, S. Tanaka, F. Terui, S. Nakazawa, S. Watanabe, and Y. Tsuda. Ryugu’s Anhydrous Ingredients and Their Spectral Link to Primitive Dust from the Outer Solar System. *Astrophys. J. Lett.*, 951(2):L33, July 2023.
- [37] B. J. R. Davidsson, H. Sierks, C. Güttsler, F. Marzari, M. Pajola, H. Rickman, M. F. A’Hearn, A. T. Auger, M. R. El-Maarry, S. Fornasier, P. J. Gutiérrez, H. U. Keller, M. Massironi, C. Snodgrass, J. B. Vincent, C. Barbieri, P. L. Lamy,

- R. Rodrigo, D. Koschny, M. A. Barucci, J. L. Bertaux, I. Bertini, G. Cremonese, V. Da Deppo, S. Debei, M. De Cecco, C. Feller, M. Fulle, O. Groussin, S. F. Hviid, S. Höfner, W. H. Ip, L. Jorda, J. Knollenberg, G. Kovacs, J. R. Kramm, E. Kührt, M. Küppers, F. La Forgia, L. M. Lara, M. Lazzarin, J. J. Lopez Moreno, R. Moissl-Fraund, S. Mottola, G. Naletto, N. Oklay, N. Thomas, and C. Tubiana. The primordial nucleus of comet 67P/Churyumov-Gerasimenko. *Astron. Astrophys.*, 592:A63, July 2016.
- [38] C. J. Bierson and F. Nimmo. Using the density of Kuiper Belt Objects to constrain their composition and formation history. *Icarus*, 326:10–17, July 2019.
- [39] Pierre Vernazza and Pierre Beck. *Composition of Solar System Small Bodies*, page 269–297. Cambridge Planetary Science. Cambridge University Press, 2017.
- [40] Sarah E. Dodson-Robinson and Peter Bodenheimer. The formation of Uranus and Neptune in solid-rich feeding zones: Connecting chemistry and dynamics. *Icarus*, 207(1):491–498, May 2010.
- [41] Ravit Helled and Peter Bodenheimer. The Formation of Uranus and Neptune: Challenges and Implications for Intermediate-mass Exoplanets. *Astrophys. J.*, 789(1):69, July 2014.
- [42] D. Baguet, A. Morbidelli, and J. M. Petit. Positions of the secular resonances in the primordial Kuiper Belt disk. *Icarus*, 334:99–109, December 2019.
- [43] David Vokrouhlický, William F. Bottke, and David Nesvorný. Capture of Trans-Neptunian Planetesimals in the Main Asteroid Belt. *Astron. J.*, 152(2):39, August 2016.
- [44] K. Tsiganis, R. Gomes, A. Morbidelli, and H. F. Levison. Origin of the orbital architecture of the giant planets of the Solar System. *Nature*, 435:459–461, May 2005.
- [45] R. Gomes, H. F. Levison, K. Tsiganis, and A. Morbidelli. Origin of the cataclysmic Late Heavy Bombardment period of the terrestrial planets. *Nature*, 435(7041):466–469, May 2005.
- [46] Sean N. Raymond and David Nesvorný. Origin and Dynamical Evolution of the Asteroid Belt. In *Vesta and Ceres. Insights from the Dawn Mission for the Origin of the Solar System*, page 227. 2022.
- [47] Alessandro Morbidelli, Ramon Brasser, Rodney Gomes, Harold F. Levison, and Kleomenis Tsiganis. Evidence from the asteroid belt for a violent past evolution of Jupiter’s orbit. *The Astronomical Journal*, 140(5):1391, oct 2010.
- [48] H. C. Bates, A. J. King, K. S. Shirley, E. Bonsall, C. Schröder, F. Wombacher, T. Fockenberg, R. J. Curtis, and N. E. Bowles. The bulk mineralogy, elemental composition, and water content of the Winchcombe CM chondrite fall. *Meteorit. Planet. Sci.*, 59(5):1006–1028, May 2024.
- [49] Anne H. Peslier, Maria Schönbachler, Henner Busemann, and Shun-Ichiro Karato. Water in the Earth’s Interior: Distribution and Origin. *Space Sci. Rev.*, 212(1–2):743–810, October 2017.
- [50] Harmon Craig. Isotopic Variations in Meteoric Waters. *Science*, 133(3465):1702–1703, May 1961.
- [51] A. Morbidelli, J. Chambers, J. I. Lunine, J. M. Petit, F. Robert, G. B. Valsecchi, and K. E. Cyr. Source regions and time scales for the delivery of water to Earth.

- Meteorit. Planet. Sci.*, 35(6):1309–1320, November 2000.
- [52] Lambrechts, M., Johansen, A., and Morbidelli, A. Separating gas-giant and ice-giant planets by halting pebble accretion. *Astron. Astrophys.*, 572:A35, 2014.
- [53] D. N. C. Lin and John Papaloizou. On the Tidal Interaction between Protoplanets and the Protoplanetary Disk. III. Orbital Migration of Protoplanets. *Astrophys. J.*, 309:846, October 1986.
- [54] Man Hoi Lee and S. J. Peale. Dynamics and Origin of the 2:1 Orbital Resonances of the GJ 876 Planets. *Astrophys. J.*, 567(1):596–609, March 2002.
- [55] A. Crida and B. Bitsch. Runaway gas accretion and gap opening versus type i migration. *Icarus*, 285:145–154, 2017.
- [56] J. F. Gonzalez, G. Laibe, S. T. Maddison, C. Pinte, and F. Ménard. The accumulation and trapping of grains at planet gaps: Effects of grain growth and fragmentation. *Planet. Space Sci.*, 116:48–56, October 2015.
- [57] Hiroshi Kobayashi, Chris W. Ormel, and Shigeru Ida. Rapid formation of saturn after jupiter completion. *The Astrophysical Journal*, 756(1):70, aug 2012.
- [58] T. Ronnet, O. Mousis, P. Vernazza, J. I. Lunine, and A. Crida. Saturn’s Formation and Early Evolution at the Origin of Jupiter’s Massive Moons. *Astron. J.*, 155(5):224, May 2018.
- [59] K. Meech and S. N. Raymond. Origin of Earth’s Water: Sources and Constraints. In Victoria S. Meadows, Giada N. Arney, Britney E. Schmidt, and David J. Des Marais, editors, *Planetary Astrobiology*, page 325. 2020.
- [60] James B. Pollack, Olenka Hubickyj, Peter Bodenheimer, Jack J. Lissauer, Morris Podolak, and Yuval Greenzweig. Formation of the Giant Planets by Concurrent Accretion of Solids and Gas. *Icarus*, 124(1):62–85, November 1996.
- [61] Pablo Benítez-Llambay, Frédéric Masset, Gloria Koenigsberger, and Judit Szulágyi. Planet heating prevents inward migration of planetary cores. *Nature*, 520(7545):63–65, April 2015.
- [62] Stephen M. Fendyke and Richard P. Nelson. On the corotation torque for low-mass eccentric planets. *Mon. Not. R. Astron. Soc.*, 437(1):96–107, January 2014.
- [63] Henrik Eklund and Frédéric S. Masset. Evolution of eccentricity and inclination of hot protoplanets embedded in radiative discs. *Mon. Not. R. Astron. Soc.*, 469(1):206–217, July 2017.
- [64] O. Chrenko, M. Brož, and M. Lambrechts. Eccentricity excitation and merging of planetary embryos heated by pebble accretion. *Astron. Astrophys.*, 606:A114, October 2017.
- [65] Sonia Cornejo, Frédéric S. Masset, and F. J. Sánchez-Salcedo. On the interaction of pebble accreting embryos with the gaseous disc: importance of thermal forces. *Mon. Not. R. Astron. Soc.*, 523(1):936–953, July 2023.
- [66] S. J. Paardekooper, C. Baruteau, A. Crida, and W. Kley. A torque formula for non-isothermal type I planetary migration - I. Unsaturated horseshoe drag. *Mon. Not. R. Astron. Soc.*, 401(3):1950–1964, January 2010.
- [67] S. J. Paardekooper, C. Baruteau, and W. Kley. A torque formula for non-isothermal Type I planetary migration - II. Effects of diffusion. *Mon. Not. R. Astron. Soc.*, 410(1):293–303, January 2011.

- [68] R. S. Gomes. The origin of the Kuiper Belt high-inclination population. *Icarus*, 161:404–418, February 2003.
- [69] H. F. Levison, A. Morbidelli, C. Vanlaerhoven, R. Gomes, and K. Tsiganis. Origin of the structure of the Kuiper belt during a dynamical instability in the orbits of Uranus and Neptune. *Icarus*, 196:258–273, July 2008.
- [70] N. A. Kaib and T. Quinn. The formation of the Oort cloud in open cluster environments. *Icarus*, 197:221–238, September 2008.
- [71] Thomas Ronnet, Olivier Mousis, and Pierre Vernazza. Pebble accretion at the origin of water in europa. *The Astrophysical Journal*, 845(2):92, aug 2017.
- [72] Hagai B. Perets and Ruth A. Murray-Clay. Wind-shearing in gaseous protoplanetary disks and the evolution of binary planetesimals. *The Astrophysical Journal*, 733(1):56, may 2011.
- [73] Tristan Guillot, Shigeru Ida, and Chris W. Ormel. On the filtering and processing of dust by planetesimals. I. Derivation of collision probabilities for non-drifting planetesimals. *Astron. Astrophys.*, 572:A72, December 2014.
- [74] Kimberley D. Supulver and D.N.C. Lin. Formation of icy planetesimals in a turbulent solar nebula. *Icarus*, 146(2):525–540, 2000.
- [75] Richard P. Nelson, John C. B. Papaloizou, Frédéric Masset, and Willy Kley. The migration and growth of protoplanets in protostellar discs. *Monthly Notices of the Royal Astronomical Society*, 318(1):18–36, 10 2000.
- [76] Bertram Bitsch, Anders Johansen, Michiel Lambrechts, and Alessandro Morbidelli. The structure of protoplanetary discs around evolving young stars. *Astron. Astrophys.*, 575:A28, March 2015.
- [77] Gennaro D’Angelo, Willy Kley, and Thomas Henning. Orbital migration and mass accretion of protoplanets in three-dimensional global computations with nested grids. *The Astrophysical Journal*, 586(1):540, mar 2003.
- [78] Anders Johansen, Mordecai-Mark Mac Low, Pedro Lacerda, and Martin Bizzarro. Growth of asteroids, planetary embryos, and kuiper belt objects by chondrule accretion. *Science Advances*, 1(3):e1500109, 2015.
- [79] N. I. Shakura and R. A. Sunyaev. Black holes in binary systems. Observational appearance. *Astron. Astrophys.*, 24:337–355, January 1973.
- [80] Lee Hartmann, Nuria Calvet, Erik Gullbring, and Paola D’Alessio. Accretion and the Evolution of T Tauri Disks. *Astrophys. J.*, 495(1):385–400, March 1998.
- [81] Alessandro Morbidelli and Aurélien Crida. The dynamics of jupiter and saturn in the gaseous protoplanetary disk. *Icarus*, 191(1):158–171, 2007.
- [82] R. von Steiger and T. H. Zurbuchen. Solar Metallicity Derived from in situ Solar Wind Composition. *Astrophys. J.*, 816(1):13, January 2016.
- [83] David Nesvorný. Dynamical Evolution of the Early Solar System. *Annu. Rev. Astron. Astrophys.*, 56:137–174, September 2018.
- [84] E. V. Pitjeva and N. P. Pitjev. Masses of the Main Asteroid Belt and the Kuiper Belt from the Motions of Planets and Spacecraft. *Astronomy Letters*, 44(8-9):554–566, August 2018.
- [85] David Vokrouhlický, William F. Bottke, and David Nesvorný. Capture of Trans-Neptunian Planetesimals in the Main Asteroid Belt. *Astron. J.*, 152(2):39, August 2016.